# $Gd_2Au_2Cd$: A $Mo_2FeB_2$-type intermetallic with ferromagnetic ordering and spin glass anomalies

S. Rayaprol and R. Pöttgen*
*Institut für Anorganische und Analytische Chemie, Westfälische Wilhelms-Universität Münster, Corrensstrasse 30, D-48149, Germany*
(Received 9 February 2006; revised manuscript received 20 March 2006; published 5 June 2006)

The ternary intermetallic compound $Gd_2Au_2Cd$, synthesized by reaction of the elements via inductive melting, is studied for its structural and physical properties. $Gd_2Au_2Cd$ crystallizes with the $Mo_2FeB_2$ type (an ordered derivative of $U_3Si_2$ structure), space group $P4/mbm$. The magnetic measurements (ac and dc susceptibility) establish magnetic ordering ($T_o$) at 110 K and have been confirmed by both transport (resistivity $\rho$;) and calorimetric (heat capacity, $C$) measurements. ac susceptibility measurements indicate "spin-glass" type anomalies below $T_o$. The nature of magnetic ordering and the low-temperature behavior in this compound have been investigated in detail.

DOI: 10.1103/PhysRevB.73.214403 PACS number(s): 75.50.Lk, 71.20.Lp

## I. INTRODUCTION

The binary compound $U_3Si_2$ has one of the simplest intergrowth structures among intermetallics compounds.[1–4] Owing to three crystallographically independent positions in the $U_3Si_2$ type structure, it is possible that ternary compounds with similar structure should also form, as seen in $Mo_2FeB_2$.[5] The structure of $Mo_2FeB_2$ is built up by an intergrowth of CsCl and $AlB_2$ related slabs of compositions MoFe and $MoB_2$. $U_2Co_2Al$ (Ref. 6) was the first compound which exhibited that the main group element and transition metal positions can be interchanged with respect to $Mo_2FeB_2$ structure. Such a crystallographic arrangement has a pronounced effect on the electron count, thus affecting the magnetic and electrical properties. Presently more than 100 compounds of the type $R_2T_2X$ ($R$=uranium or rare earth metals, $T$=transition metal, $X$=main group metal) with ordered $U_3Si_2$ structure are known, and many of these compounds exhibit interesting physical properties. The structure-property relations in these compounds have been recently reviewed.[7]

Among the gadolinium intermetallics with $Mo_2FeB_2$ type structure $Gd_2Au_2In$ and $Gd_2Cu_2In$ order ferromagnetically at 83 and 85.5 K, respectively,[8,9] whereas $Gd_2Pd_2In$ orders antiferromagnetically at 65 K.[10] Among the $R_2T_2Cd$ intermetallics, $Gd_2Ni_2Cd$ is known to exhibit antiferromagnetic ordering at 65 K, but has an orthorhombic $Mn_2AlB_2$ type structure (space group $Cmmm$)[11] with a different intergrowth of the CsCl and $AlB_2$ slabs.

The present study has been motivated by the fact that gadolinium intermetallics have promising application potentials owing to large magnetocaloric effect (MCE) and giant magnetoresistance (GMR) observed in several compounds.[12–15] Another reason has been the observation of several interesting phenomena, such as anomalies in heat capacity and magnetoresistance, noncollinear amplitude modulation, magnetic precursor effects, and giant magnetostriction, etc., in gadolinium intermetallics.[16–24] Magnetic clusters were observed in amorphous, spin-glass La-Gd-Au alloys.[25]

Though there are many studies on the physical properties of $R_2T_2In$ and $R_2T_2Sn$ intermetallics,[7] there are very few reports on the physical properties of $R_2T_2X$ compounds with $X$=Cd (Refs. 11, 26, and 27). It is difficult to prepare the Cd containing 221 intermetallics by arc-melting the pure metals because of the low boiling point of Cd. These syntheses have to be carried out by induction melting, in a sealed tantalum or niobium crucibles, using high-frequency induction furnaces.[26–29] Using the synthesis method referred above, we have successfully synthesized $Gd_2Au_2Cd$ which crystallizes in $Mo_2FeB_2$ type structure (space group $P4/mbm$). We present the physical properties of this intermetallic herein.

## II. EXPERIMENTAL DETAILS

The starting materials for the synthesis of the title compound were ingots of gadolinium (Johnson Matthey), thin sheets of gold (Heraeus), and cadmium rod pieces (Johnson Matthey), all with purity better than 99.9%. The large pieces of gadolinium were cut into smaller pieces, washed with $n$-hexane and preserved in Schlenk tubes. $n$-hexane used here has been dried over sodium wire. The elements were taken in the atomic ratio 2:2:1 and sealed in a tantalum tube of about 1 $cm^3$ volume, under an argon atmosphere of approximately 600 mbar pressure. The argon was purified over titanium sponge (870 K), silica gel, and molecular sieves. Details about the arc-welding technique are given in Ref. 30. The sealed tantalum tube placed in a water-cooled quartz sample chamber of a high-frequency furnace (Hüttinger Elektronik, Freiburg TIG 1.5/300) under flowing argon (~600 mbar) was brought to approximately 1500 K for 1 min and subsequently annealed at ~900 K for another 2 h by inductive heating. The product could be easily separated from the tantalum tube. To improve the homogeneity in the sample, the product thus obtained was further ground, pelletized, and annealed in an evacuated sealed quartz tube for 4 weeks at 973 K.

The purity of the sample was checked through a Guiner powder pattern with Cu-$K_{\alpha 1}$ radiation and using $\alpha$-quartz ($a$=491.30, $c$=540.46 pm) as an internal standard. Resistivity ($\rho$), magnetic ($\chi_{dc}$, $\chi_{ac}$ and high-field magnetization), and specific heat ($C$) measurements were carried out on a Quantum Design Physical Property Measurement System (PPMS) using resistivity, AC Measurement System (ACMS), and heat capacity options, respectively.

 

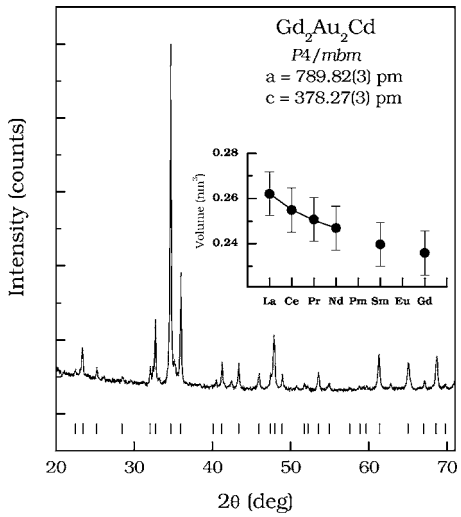


FIG. 1. Powder XRD pattern for $Gd_2Au_2Cd$. The expected peaks are marked by vertical lines. In the inset, the course of the unit cell volume as a function of the rare-earth atom is shown. The error bars indicate the standard deviation of the data points.

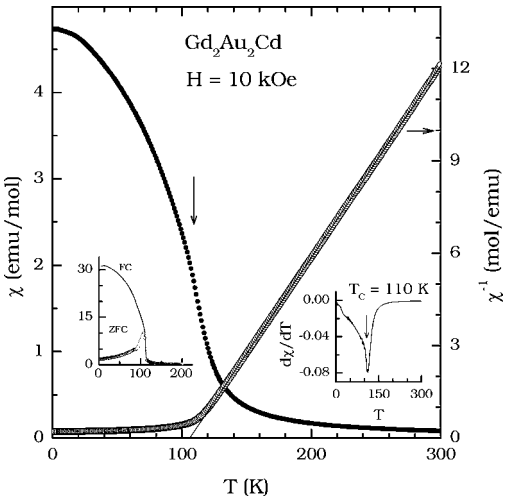


FIG. 2. dc susceptibility ($\chi$) and inverse ($\chi^{-1}$) susceptibility measured under $H=10$ kOe. The straight line passing through the data points is the extrapolation of Curie-Weiss fit from the paramagnetic region. The derivative of $\chi$ ($=M/H$) is shown as an inset in the figure, to precisely determine the ordering temperature. In another inset, low field ($H=100$ Oe) susceptibility is shown for ZFC and FC state of the sample.

The bulk sample was carefully analyzed in a Leica 420 I scanning electron microscope equipped with an Oxford EDX analyzer. The sample was embedded in a metacrylate matrix and polished with different silica and diamond pastes and left unetched for the analyses in the scanning electron microscope in backscattering mode. $GdF_3$, Au, and Cd have been used as standards for the energy dispersive x-ray (EDX) measurements. The various point analyses revealed a composition of 40±2 at. % Gd: 41±2 at. % Au: 19±2 at. % Cd were in good agreement with the ideal composition. No impurity elements heavier than sodium (limit of the spectrometer) have been observed. Also no tantalum contaminations from the container material were evident.

## III. RESULTS

### A. Structure

The x-ray diffraction (XRD) powder pattern of $Gd_2Au_2Cd$ shows that the compound has a tetragonal unit cell with $Mo_2FeB_2$ type structure, space group $P4/mbm$. The experimental powder pattern along with expected peak positions is shown in Fig. 1. The cell constants of $a=789.82(3)$, $c=378.27(3)$ pm, were calculated by a least-squares refinements of the powder data and the correct indexing of the profile was carried out using an intensity calculation.[31] Although the EDX analyses of the sample revealed no impurity phases, one very weak additional reflections around $2\theta=42°$ occurred in the powder diagram, probably due to an oxidation or hydrolysis of the fine-grained powder used for the x-ray diffraction experiment.

In the inset of Fig. 1, we have plotted the course of the cell volumes for the $RE_2Au_2Cd$ ($RE$=rare earth) series. As expected from the lanthonoid contraction, volume decreases with increasing $4f$ electrons, up to $RE$=Gd. The attempts to synthesize compounds with rare earths above Gd in the $RE_2Au_2Cd$ series have not been successful so far. For a detailed discussion on the crystal chemistry of the $RE_2Au_2Cd$ series, we refer to the original work[29] and the review article.[7]

### B. Physical properties

The sample was enclosed in a gelatin capsule and taken up for the magnetic measurements. In Fig. 2, we show the dc susceptibility ($\chi$) as a function of temperature measured under an applied field of 10 kOe. $\chi$ increases linearly with decreasing temperature and exhibits a sudden upturn around 110 K, as if undergoing ferromagnetic ordering. Below 110 K, $\chi$ increases with a tendency to saturate at lower temperatures. In the inset of Fig. 2 we have plotted the first derivative of $\chi$ to get a precise value of the ordering temperature. The inverse susceptibility ($\chi^{-1}$) deviates from Curie-Weiss law just below 110 K. From the high-temperature fit of $\chi^{-1}$, we obtain the paramagnetic Curie temperature ($\theta_p$) of 106.1(3) K and effective Bohr magneton number ($\mu_{eff}$) of 8.01(1) $\mu_B$/Gd mol, which is in close agreement with the expected value of 7.94 $\mu_B$/Gd mol for free $Gd^{3+}$ ion.[32] The positive sign of $\theta_p$ indicates ferromagnetic interactions. In another inset of Fig. 2, low-field ($H=100$ Oe) susceptibility is plotted for zero field cooled (ZFC) and field cooled (FC) state of the sample. The $\chi$(T) measured in ZFC and FC bifurcate at 110 K.

The resistivity of the bulk sample was measured using the four-probe resistivity method. Four thin copper wires were attached to the sample using silver epoxy. The sample was attached to the platform using thermally conducting germanium varnish. In Fig. 3 we have plotted the resistivity of $Gd_2Au_2Cd$ measured from 5 to 300 K. The sample is metallic in the entire temperature range. To show the linear behavior of $\rho$, we have drawn straight lines passing through the data points. $\rho$ decreases linearly with decreasing temperature

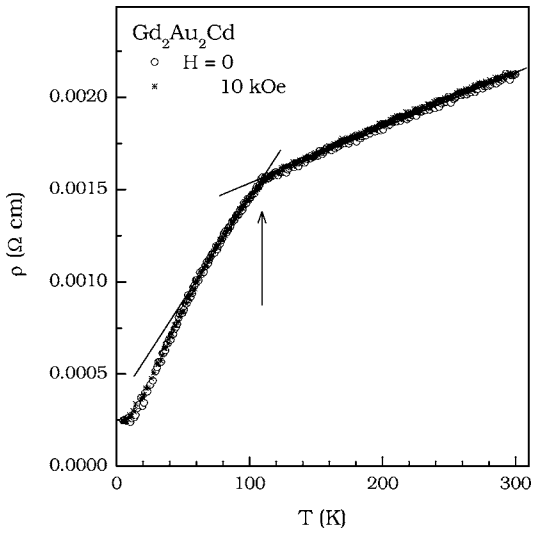


FIG. 3. Specific resistivity as a function of temperature for $Gd_2Au_2Cd$ measured in $H=0$ and 10 kOe. The vertical arrow shows the change of slope (which coincides with the ordering temperature).

up to 110 K, where it undergoes ordering and decreases rapidly owing to the decrease of spin-disorder scattering. $\rho$ is linear in the temperature range 60–110 K; however, below 60 K it varies roughly as $\propto T^{3/2}$. High value of specific resistivity of the order of 2 m$\Omega$ cm at room temperature indicates that $Gd_2Au_2Cd$ is a poor metallic conductor. The vertical arrow in Fig. 3 shows the temperature at which ordering takes place. We have also measured resistivity in the presence of externally applied magnetic fields of 5 kOe and 10 kOe. In Fig. 3 we have shown the $\rho(T)$ measured under a steady field of 10 kOe. There is almost no effect of $H$ on the behavior of $\rho$. Magnetoresistance calculated as $\Delta\rho/\rho$, is less than 1% around the ordering temperature.

There is a sharp peak exhibiting $\lambda$ anomaly, around 110 K in the plot of $C$ versus $T$, shown in Fig. 4. Heat capacity of the nonmagnetic $La_2Au_2Cd$ up to 80 K was reported by us earlier,[27] and for the present study we have remeasured the same piece of the sample up to 150 K, to get the magnetic part of the heat capacity for $Gd_2Au_2Cd$. In the top panel of Fig. 4, we have plotted the $C$ data for $La_2Au_2Cd$, for the entire range of temperature. The magnetic part of heat capacity ($C_m$) is plotted in the bottom panel of the Fig. 4. The ordering around 110 K is clearly seen in $C_m(T)$ also. The inset of this panel shows the linearity of $C_m/T$ as a function of $T^2$ at low temperatures. We observed small anomalies in $C_m(T)$ around 90, 60, and 30 K and may have arisen because of a small inhomogeneity in the sample, as we did not see any anomaly around these temperatures in other measurements. However, the main point of interest is the magnetic ordering in $Gd_2Au_2Cd$ at 110 K. At low temperatures ($T<10$ K), $C_m/T$ varies linearly with $T^2$, yielding the values of coefficient of the electronic specific heat, $\gamma=92(1)$ mJ/mol $K^2$ and a very small value of the coefficient of thermal expansion, $\beta=3.2(5)$ mJ/mol $K^4$.

A theoretical model within the framework of mean-field theory was given by Rotter *et al.*[22] to analyze the specific

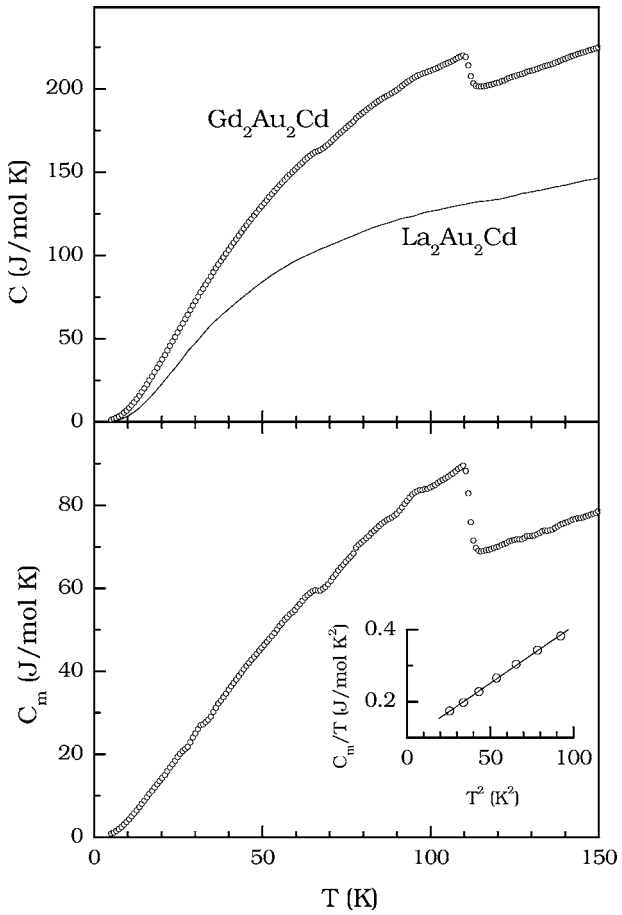


FIG. 4. Heat capacity of $Gd_2Au_2Cd$ and $La_2Au_2Cd$. The magnetic part of heat capacity for $Gd_2Au_2Cd$, i.e., $C_m$ obtained after subtracting the lattice part using the $La_2Au_2Cd$ data, is shown in the bottom pane. In the inset, we show the linear variation of $C_m/T$ vs $T^2$ at low temperatures.

heat of magnetically ordered systems. The authors have developed a theoretical model for noncollinear amplitude-modulated (NCAM) systems, considering the anisotropy of the exchange interaction. Amplitude-modulated (AM) and equal-moment (EM) orders are derived as special case of this model. According to this model, the specific heat near the ordering temperature shows a discontinuity that corresponds to the size of the derivative of the ordered magnetic moment with respect to time ($t$). The jump in molar heat capacity at the ordering temperature ($T_N$ in the case of said theory) may vary between 13.43 J/mol K and 20.15 J/mol K for AM and EM magnetic structures respectively. The magnetic contribution to the molar heat capacity near the magnetic ordering temperature for $Gd_2Au_2Cd$ is close to 20 J/mol K, which is in good agreement with the values expected for EM magnetic structures. Also, the theoretical model given by Rotter *et al.* predicts that ferromagnetic and simple antiferromagnetic case give specific heat values as expected for EM order. The structural information derived for isostructural $RE_2T_2Cd$ intermetallics confirm the presence of only one *RE* site (Gd in this case) in these compounds; therefore, either AM or simple collinear EM order can be predicted in this case. From the magnetic measurements the antiferromagnetic or-

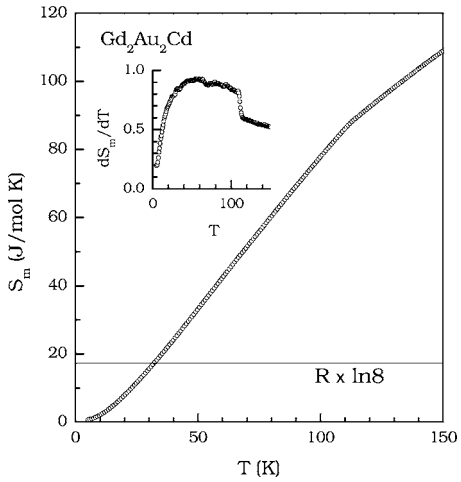


FIG. 5. Magnetic entropy of $Gd_2Au_2Cd$ plotted as a function of temperature. The inset shows the derivative of $S_m$, to highlight the change in entropy above the ordering temperature. The horizontal line is drawn to show the $R \ln 8$ value.

dering can be ruled out, and hence EM magnetic structure is most likely the case for $Gd_2Au_2Cd$.

In Fig. 5, we have plotted the changes in the magnetic entropy ($S_m$) as a function of temperature. $S_m$ does not saturate above $T_o$ but increases in the entire temperature range. However $S_m$ changes slope just above $T_o$, which can be clearly seen in the plot of $dS_m/dT$ (inset). From the applications point of view, to qualify as efficient magnetocaloric (MCE) compounds, ferromagnetic material should exhibit large MCE at higher temperatures and for smaller intervals of $\Delta H$. In order to explore the effect of magnetic field on the ferromagnetic ordering of $Gd_2Au_2Cd$, and to see if it might be a suitable MCE compound, we measured $C(T)$ under an applied field of strength 10 kOe (Fig. 6). The magnitude of the peak is suppressed by the application of the field and the ordering temperature shifts down from 110 (for $H=0$) to 107 K ($H=10$ kOe). The inset in Fig. 6 highlights the difference in the $C(T)$ around $T_o$ for measurements carried out under $H=0$ and 10 kOe. In Fig. 7, we have plotted the total entropy of the system, in $H=0$ and 10 kOe. The application of the magnetic field has very little effect on the total entropy. The change in total entropy ($\Delta S$) as a consequence of the application of a field of 10 kOe is shown as an inset in Fig. 7. The negative sign of $\Delta S$, and its caretlike shape, shows the ferromagnetic nature of the ordering in $Gd_2Au_2Cd$.[12] The maximum of $\Delta S$ at 110 K is about 0.75 J/mol K, for a change in field ($\Delta H$) from 0 to 10 kOe.

Plotted in Fig. 8 is the magnetization, $M(H)$, of $Gd_2Au_2Cd$ at several temperatures spanning $T_o$ up to field strengths of 80 kOe. In the magnetically ordered state, i.e., at $T<T_o$, $M$ varies sluggishly with $H$ as in an antiferromagnet, and with a tendency to saturate at higher fields. For $T=5$ K, the moment value at 80 kOe is 6.80 $\mu_B$/Gd atom, in close agreement with calculated saturation moment for $Gd^{3+}$ ($g \times J=7.0$). The saturation moment value decreases with increasing temperature. At $T>T_o$, we also observe gradual increase in $M$ with increasing field, without saturation up to 80 kOe. It is also important to note here that since there is no

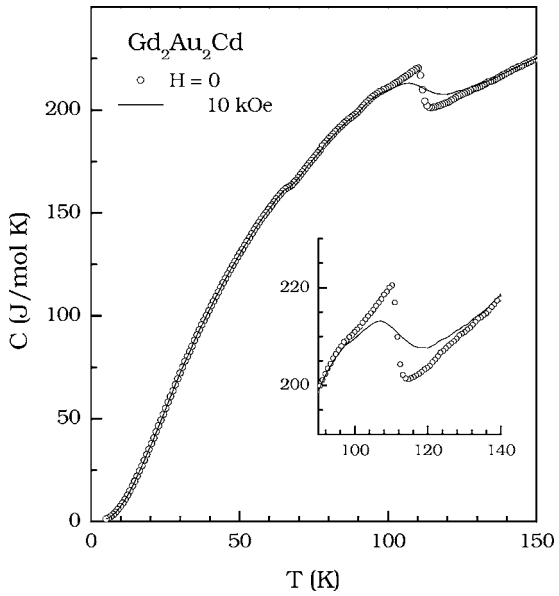


FIG. 6. Heat capacity for $Gd_2Au_2Cd$ measured in $H=0$ and 10 kOe. The inset highlights the change in $C(T)$ around the ordering temperature.

hysteresis observed in the up (increasing field) and down (decreasing field) cycles, we have only plotted the up cycle for all temperatures. It is interesting to compare the magnetization behavior of $Gd_2Au_2Cd$ with the similar features observed in amorphous $La_{64}Gd_{16}Au_{20}$, which is a spin glass with magnetic clusters.[25]

One of the methods for determining the presence of ferromagnetic ordering is the Arrott plot.[33] The Arrott's method is based on the Weiss molecular-field theory which shows that the Curie temperature is generally indicated by the proportionality of third power of magnetization ($M^3$) to the internal field ($H$). In the plot of $M^2$ versus $H/M$, when $M^2 \rightarrow 0$, the intercept on the $H/M$ axis gives $1/\chi$ according to the Arrott's criterion. The temperature at which $1/\chi$ goes to 0

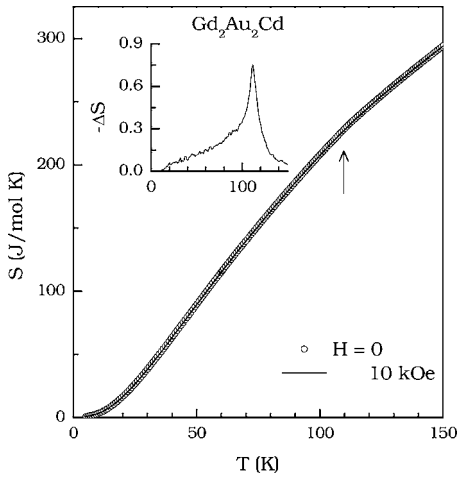


FIG. 7. The change in total entropy of the system is plotted as a function of temperature for $H=0$ and 10 kOe. The inset shows magnetocaloric effect ($\Delta S$) around the ordering temperature. The vertical arrow indicates the ordering temperature.

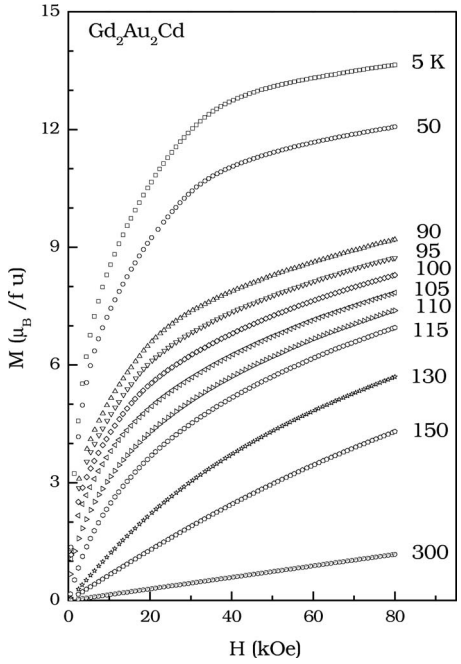


FIG. 8. Magnetization per formula unit as a function of applied field for various temperatures.

is the Curie temperature. In Fig. 9, we have plotted $M^2$ versus $H/M$ using the data from Fig. 8. For $T<T_o$, the slope from the linear region at the higher fields has a positive value, and as $T\sim T_o$, the intercept goes to zero, and above $T_o$, the slope is negative, which confirms the presence of spontaneous magnetization in $Gd_2Au_2Cd$, which is associated with the ferromagnetic ordering we observed at 110 K.

Changing temperature at fixed fields (susceptibility) leads only to rather small irreversibility effects; changing the field at fixed temperatures below the spin-freezing temperature

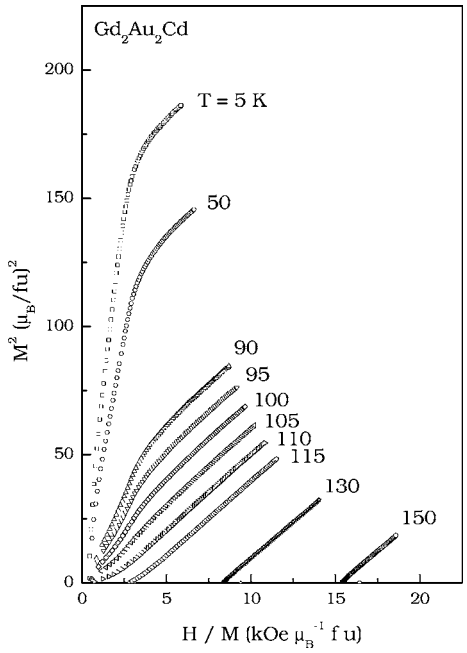


FIG. 9. Arrott's plot using the data of Fig. 8.

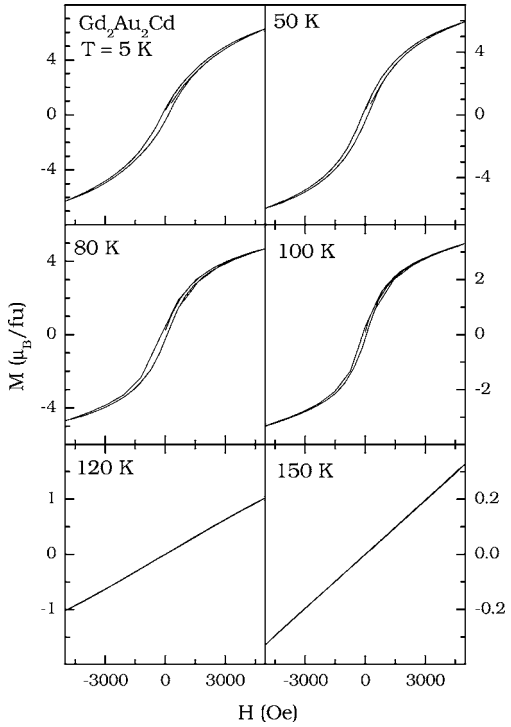


FIG. 10. Magnetization loops as a function of varying field, plotted for different temperatures.

($T_f$) of a spin glass gives rise to pronounced irreversibility. In particular if one cycles the field from positive to negative values and back, one observes hysteresis phenomena as in ferromagnets.[34] However, the shape of the hysteresis loop depends on the history of the sample. The magnetization $M_{ZFC}$ $(H)$ has a characteristic S-shaped form. This S-shaped behavior is seen in metallic spin glasses, such as AuFe, CuMn, $Eu_xSr_{s-x}S$, at temperatures below $T_f$.[34,35]

In order to probe the low-field behavior of $Gd_2Au_2Cd$ at temperatures below and above $T_o$, we have measured hysteresis at various temperatures across $T_o$, and shown in Fig. 10. The characteristic S-shaped $M(H)$ loop of metallic spin glasses can be seen at $T$=5, 50, 80, and 100 K and these curves have small hysteresis also. The $MH$ loops of $Gd_2Au_2Cd$ look similar to those of AuFe, i.e., narrow and flat and antisymmetric around the origin.[34,35] Above the ordering temperature (110 K), i.e., at 120 and 150 K, the $MH$ loops varies linearly with $H$, as expected for the paramagnetic state.

Binder and Young[34] predict complicated behavior in systems where spin glass and ferromagnetic ordering compete and in which states with mixed ordering can be produced. We measured isothermal remanent magnetization ($M_{IRM}$) at temperatures below and above $T_o$, to see if $Gd_2Au_2Cd$ has the relaxation process usually associated with spin glasses. After zero field cooling from higher temperatures to the temperatures at which $M_{IRM}$ is measured ($T$=5, 90, and 120 K), a field of 5 kOe was applied for 5 min and then switched off. As soon as the field reached zero value, $M_{IRM}$ was measured for a definite period of time. As can be clearly seen in Fig. 11, the relaxation behavior at 5 K (far below $T_o$) and 90 K (just below $T_o$) is somewhat similar but complex. $M_{IRM}$ de-

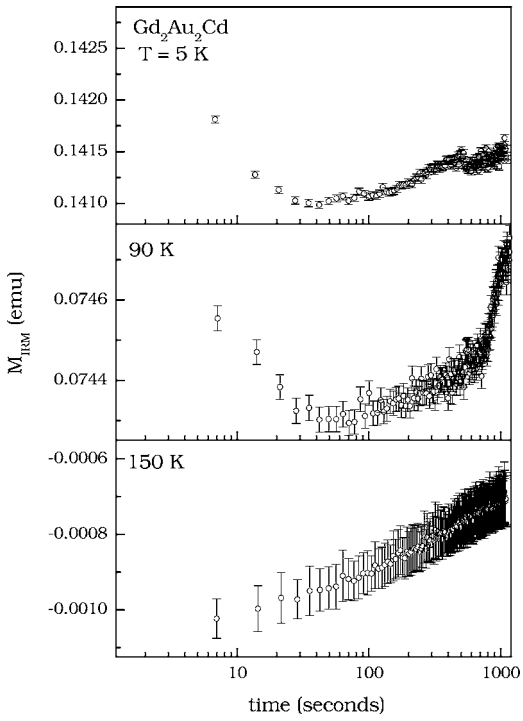


FIG. 11. Isothermal remanent magnetization measured at $T=5$, 90, and 120 K, plotted as a function of time (in seconds, on a log scale). See text for details of the experiment.

creases logarithmically for few seconds only and then tries to level off at a higher value. However, at 120 K (just above $T_o$) there is no relaxation at all.

The investigation of linear and nonlinear susceptibilities is an important experimental tool in studying transitions

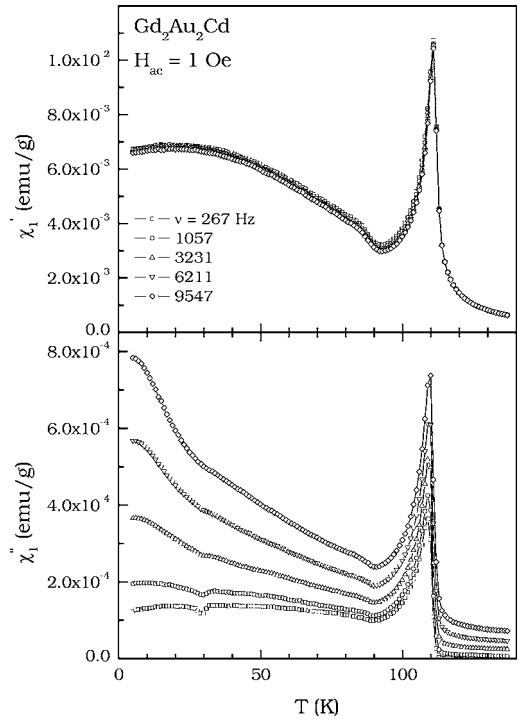


FIG. 12. Real and imaginary part of the linear susceptibility for $Gd_2Au_2Cd$.

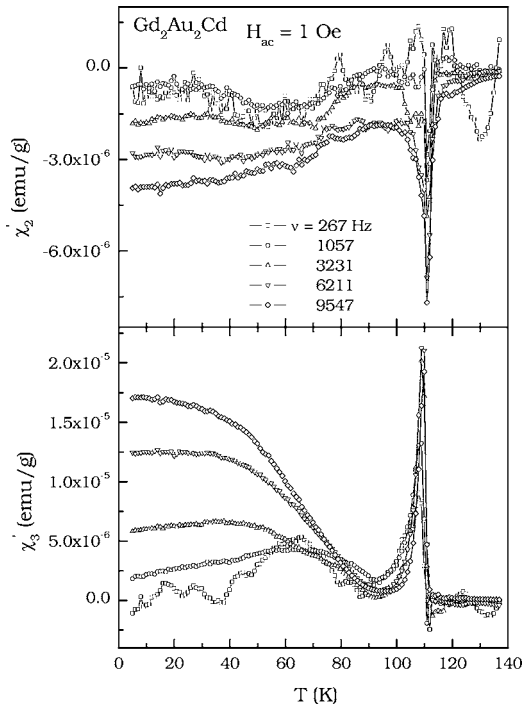


FIG. 13. Real part of the nonlinear susceptibility measured at second and third harmonics.

from the paramagnetic (PM) to the ferromagnetic (FM) state, as well as in the study of compounds exhibiting PM-FM-SG (spin glass) transitions or so-called reentrant spin-glass (RSG) transition.[36–44] To gain further insight into the low-temperature behavior of $Gd_2Au_2Cd$, we have measured the linear ($\chi_1$) and nonlinear susceptibilities ($\chi_2$ at second, and $\chi_3$ at third harmonics). In Fig. 12, we show the real (disper-

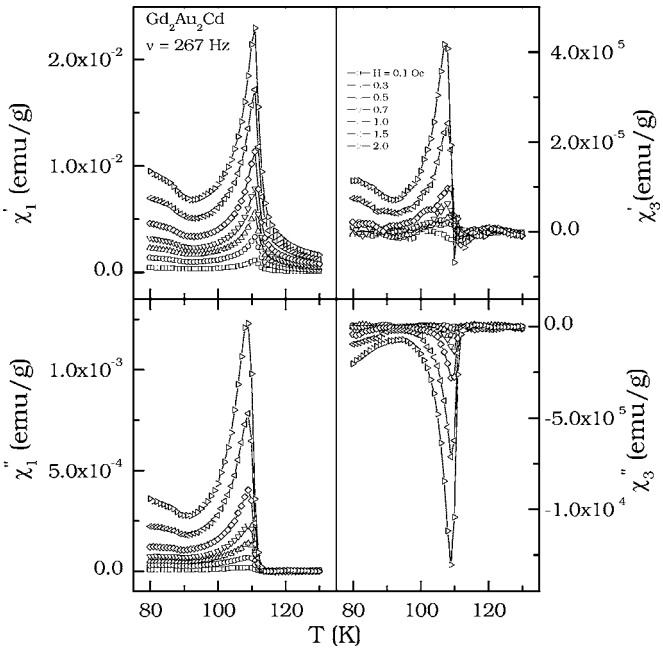


FIG. 14. Real and imaginary part of the linear ($\chi_1$) and nonlinear ($\chi_3$) susceptibilities measured at a frequency of 267 Hz and at different ac amplitudes.

sion) and imaginary (absorption) part of the linear susceptibility measured with an ac field (amplitude) of 1 Oe. At all frequencies measured, $\chi_1$ exhibits a sharp peak at 110 K in real ($\chi_1'$) and imaginary ($\chi_1''$) part. The temperature at which the linear susceptibility exhibits a peak is consistent with dc susceptibility and other measurements. The features of ac susceptibility are broadly in agreement with the susceptibilities of a ferromagnet coexisting with reentrant spin-glass transition.[37,41] The $\chi_1''$ exhibits broad peak at lower temperatures as if undergoing a transition below 5 K. In Fig. 13 we show the real part of the nonlinear susceptibilities ($\chi_2$ and $\chi_3$). The observation of peaks in $\chi_1''$ and $\chi_3'$ are consistent with the features of a spin-glass system. It may be recalled here that a peak in $\chi_2$ should appear only if there is spontaneous magnetization. In Fig. 13, we can clearly see a peak around 110 K for $\chi_2$. The presence of $\chi_2$ supports the existence of a FM moment, coinciding with the observations made from the Arrott's plot. In order to verify if there is any field dependence on linear or nonlinear susceptibilities, we have measured $\chi_1$ and $\chi_3$ at different ac amplitudes for a frequency of 267 Hz. The plot is shown in Fig. 14. The presence of peak at 110 K is further confirmation of coexistence of ferromagnetic ordering with RSG state.

To conclude, we have successfully synthesized the ternary intermetallic $Gd_2Au_2Cd$ compound and studied its physical properties. The compound exhibits ferromagnetic ordering at 110 K, followed by a spin-glass state. We strongly feel that the present study will stimulate further work on this interesting compound to understand its magnetic behavior in detail.

## ACKNOWLEDGMENTS

We thank C. P. Sebastian for the EDX analyses. This work was supported by the Deutsche Forschungsgemeinschaft through the priority program SPP 1166 "Lanthanoidspezifische Funktionalitäten in Molekül und Material." S.R. is indebted to the Alexander von Humboldt Foundation for financial support.

*Corresponding author. Email address: pottgen@uni-muenster.de

[1] W. H. Zachariasen, Acta Crystallogr. **2**, 94 (1949).
[2] K. Remschnig, T. Le Bihan, H. Nöel, and P. Rogl, J. Solid State Chem. **97**, 391 (1992).
[3] P. Villars and D. L. Calvert, *Pearson's Handbook of Crystallographic Data for Intermetallic Phases*, 2nd ed. (American Society for Metals, Materials Park, OH, 1991).
[4] Ch. Druska, Th. Doert, and P. Böttcher, Z. Anorg. Allg. Chem. **622**, 401 (1996).
[5] W. Rieger, H. Nowotny, and F. Benesovsky, Monatsh. Chem. **95**, 1502 (1964).
[6] A. O. Sampaio, E. Santa Marta, H. L. Lukas, and G. Petzow, J. Less-Common Met. **14**, 472 (1968).
[7] M. Lukachuk and R. Pöttgen, Z. Kristallogr. **218**, 767 (2003).
[8] F. Hulliger, J. Alloys Compd. **232**, 160 (1996).
[9] I. R. Fisher, Z. Islam, and P. C. Canfield, J. Magn. Magn. Mater. **202**, 1 (1999).
[10] M. Giovannini, H. Michor, E. Bauer, G. Hilscher, P. Rogl, and R. Ferro, J. Alloys Compd. **280**, 26 (1998).
[11] F. Canepa, S. Cirafici, F. Merlo, M. Pani, and C. Ferdeghini, J. Magn. Magn. Mater. **195**, 646 (1999).
[12] See, for instance, K. A. Gschneidner, Jr. and V. K. Pecharsky, Annu. Rev. Mater. Sci. **30**, 387 (2000); K. A. Gschneidner, Jr., V. K. Pecharsky, and A. O. Tsokol, Rep. Prog. Phys. **68**, 1475 (2005).
[13] E. Brück, J. Phys. D **38**, R381 (2005).
[14] K. Sengupta, S. Rayaprol, and E. V. Sampathkumaran, Europhys. Lett. **69**, 454 (2005).
[15] K. Sengupta, K. K. Iyer, and E. V. Sampathkumaran, Phys. Rev. B **72**, 054422 (2005).
[16] M. J. Parsons, J. Crangle, K.-U. Neumann, and K. R. A. Ziebeck, J. Magn. Magn. Mater. **184**, 184 (1992).
[17] E. V. Sampathkumaran and R. Mallik, *Concepts in Correlations*, edited by A. Hewson and V. Zlatic (Kluwer Academic, Dordrecht, 2003), Vol. 110, p. 666.
[18] E. V. Sampathkumaran and I. Das, Physica B **223&224**, 149 (1996).
[19] S. N. Kaul, Pramana, J. Phys. **60**, 505 (2003).
[20] E. Gratz and A. Lindbaum, J. Magn. Magn. Mater. **177-181**, 1077 (1998).
[21] R. Mallik and E. V. Sampathkumaran, Phys. Rev. B **58**, 9178 (1998).
[22] M. Rotter, M. Loewenhaupt, M. Döerr, A. Lindbaum, and H. Michor, Phys. Rev. B **64**, 014402 (2001).
[23] M. D. Kuz'min, Phys. Rev. B **46**, 8219 (1992).
[24] R. P. Pinto, J. B. Sousa, F. C. Correia, J. P. Araujo, M. E. Braga, A. M. Pereira, L. Morellon, P. A. Algarabel, C. Magen, and M. R. Ibarra, J. Magn. Magn. Mater. **290&291**, 661 (2005).
[25] S. J. Poon and J. Durand, Phys. Rev. B **18**, 6253 (1978).
[26] D. Niepmann, R. Pöttgen, B. Künnen, and G. Kotzyba, J. Solid State Chem. **150**, 139 (2000).
[27] S. Rayaprol and R. Pöttgen, Phys. Rev. B **72**, 214435 (2005).
[28] R. Pöttgen, A. Fugmann, R.-D. Hoffmann, U. Ch. Rodewald, and D. Niepmann, Z. Naturforsch., B: Chem. Sci. **55**, 155 (2000).
[29] R. Mishra, R. Pöttgen, R.-D. Hoffmann, D. Kaczorowski, H. Piotrowski, P. Mayer, C. Rosenhahn, and B. D. Mosel, Z. Anorg. Allg. Chem. **627**, 1283 (2001).
[30] R. Pöttgen, Th. Gulden, and A. Simon, GIT Labor-Fachz. **43**, 133 (1999).
[31] K. Yvon, W. Jeitschko, and E. Parthe, J. Appl. Crystallogr. **10**, 73 (1977).
[32] J. Jensen and A. R. Mackintosh, in *Rare Earth Magnetism: Structures and Excitations* (Clarendon Press, Oxford, 1991).
[33] A. Arrott, Phys. Rev. **108**, 1394 (1957).
[34] K. Binder and A. P. Young, Rev. Mod. Phys. **58**, 801 (1986).
[35] J. J. Prejean and J. Souletie, J. Phys. (Paris) **41**, 1335 (1980).
[36] A. Chakravarti, R. Ranganathan, and C. Bansal, Solid State Commun. **82**, 591 (1992).
[37] M. Suzuki, Prog. Theor. Phys. **58**, 1151 (1977).
[38] T. Taniguchi, Y. Miyako, and J. L. Tholence, J. Phys. Soc. Jpn. **54**, 220 (1985).
[39] B. R. Coles, Philos. Mag. B **49**, L21 (1984).

[40] H. P. Kunkel and G. Williams, J. Magn. Magn. Mater. **75**, 98 (1988).
[41] A. Chakravarti, R. Ranganathan, and S. B. Roy, Phys. Rev. B **46**, 6236 (1992).
[42] S. Nair and A. Banerjee, Phys. Rev. B **68**, 094408 (2003).
[43] S. Mukherjee, R. Ranganathan, A. Chakravarti, and S. Sil, J. Magn. Magn. Mater. **224**, 210 (2001).
[44] V. Tsurkan, J. Hemberger, M. Klemm, S. Klimm, A. Liodl, S. Horn, and R. Tidecks, J. Appl. Phys. **90**, 4639 (2001).